Evaluation of the effect of sporadic-E on high frequency radio wave propagation in the Arctic

Cameron, T. G.; Fiori, R. A.D.; Themens, D. R.; Warrington, E. M.; Thayaparan, T.; Galeschuk, D.

DOI:
10.1016/j.jastp.2022.105826

Journal of Atmospheric and Solar–Terrestrial Physics 228 (2022) 105826

Contents lists available at ScienceDirect

Journal of Atmospheric and Solar-Terrestrial Physics

journal homepage: www.elsevier.com/locate/jastp

Research Paper

Evaluation of the effect of sporadic-E on high frequency radio wave propagation in the Arctic

T.G. Cameron [a,*], R.A.D. Fiori [a], D.R. Themens [b,c], E.M. Warrington [d], T. Thayaparan [e], D. Galeschuk [a,f]

[a] Canadian Hazards Information Service, Natural Resources Canada, Ottawa, Ontario, Canada
[b] Department of Physics, University of New Brunswick, Fredericton, NB, Canada
[c] Space Environment and Radio Engineering Group, School of Engineering, University of Birmingham, Birmingham, B15 2TT, United Kingdom
[d] School of Engineering, University of Leicester, University Road, Leicester, LE1 7RH, United Kingdom
[e] Defense Research and Development Canada, Ottawa Research Centre, 3701 Carling Avenue, K1A 0Z4, Ottawa, Ontario, Canada
[f] Department of Physics and Engineering Physics, University of Saskatchewan, 116 Science Place, S7N 5E2, Saskatoon, Saskatchewan, Canada

ARTICLE INFO

Key points:
High frequency radio wave propagation
Sporadic-E
Ionosphere
High-latitude

ABSTRACT

High Frequency (HF) radio propagation, and applications such as Over-The-Horizon Radar (OTHR), is sensitive to ionospheric disturbances caused by space weather. Improved ionospheric modelling and monitoring techniques for the high-latitude and polar regions supports high quality OTHR long-range surveillance. One such ionospheric disturbance is Sporadic-E, a phenomenon in which a thin enhancement in E-region (approximately 90–150 km altitude) electron density acts as a strong reflector of HF radio waves. In this study, we perform a case study of the effect a sporadic-E layer has on HF radio propagation for a layer that was detected over Eureka on July 11, 2012. We study this event using HF radio receiver measurements for a path intersecting the layer, simultaneous ionosonde measurements of the layer, and a series of ray traces through a model ionosphere containing a model of the sporadic-E layer. Utilizing these measurements and simulations, we show how sporadic-E can aid HF radio propagation in some cases, and show that a simple Gaussian sporadic-E model can replicate real HF radio measurements. We also comment on how sporadic-E could affect OTHR operation.

1. Introduction

Ionospheric disturbances resulting from magnetosphere-ionosphere-atmosphere coupling processes occurring both on a regular basis, and enhanced by space weather contributions originating from the sun, potentially impact high frequency (3–30 MHz; HF) radio wave propagation (Cannon et al., 2013; Coyne, 1979; Davies, 1990, Goodman, 1992; Hunsucker and Hargreaves, 2003; Newell et al., 2001). Electron density is a key ionospheric characteristic governing HF radio wave propagation dictating at what frequency radio waves are absorbed by the D-region ionosphere (e.g., Zawdie et al., 2017), reflected from or refracted through the E and F-region ionosphere (Davies, 1990), or transmitted through the ionosphere (e.g., satellite communications [SATCOM]). The band of HF frequencies at which HF radio wave propagation is possible for a given HF radio system is bounded by the lowest useable frequency (LUF) and maximum useable frequency (MUF) (Davies, 1990). Frequencies below the LUF are absorbed in the D-region ionosphere, and frequencies above the MUF penetrate the ionosphere and travel out to space. The LUF and MUF vary according to the level of ionization, primarily controlled by photoionization due to solar radiation, and experience predictable daily and seasonal variations (Davies, 1990). Since different radio receivers have varying levels of sensitivity, LUF is a system dependent quantity. D-region absorption, and subsequently the LUF also depends on the thermosphere/mesosphere neutral density and plasma temperature. Ionospheric disturbances caused by localized or large-scale enhancements of the ionospheric electron density thereby shift the LUF and/or MUF and alter the band of useable frequencies.

Over-the-horizon radar (OTHR), used for long-range surveillance (Thayaparan et al., 2018; Cervera et al., 2018), relies on HF radio wave propagation, and is therefore sensitive to changes in the ionospheric electron density profile. Radio wave propagation modelling, or ray tracing, supports OTHR by predicting propagation paths to accurately range targets and optimize frequency selection (Thayaparan et al., 2018;

* Corresponding author.
E-mail address: taylor.cameron@NRCan-RNCan.gc.ca (T.G. Cameron).

https://doi.org/10.1016/j.jastp.2022.105826
Received 24 September 2021; Received in revised form 7 December 2021; Accepted 7 January 2022
Available online 13 January 2022

2019a; 2019b, 2020). This paper employs the High-Latitude Ionospheric Propagation Lab (HIPLAB) 3-D ray tracer toolbox to study the propagation of radio waves through the ionosphere. The University of Leicester developed HIPLAB with funding and support from Defence Research and Development Canada's (DRDC) All Domain Situational Awareness (ADSA) program (Warrington, 2020). HIPLAB is based on Warrington et al. (2016) as described in Zaalov et al. (2003, 2005). This model builds on Jones and Stephenson (1975) by incorporating the Empirical Canadian High Arctic Ionospheric Model (E-CHAIM) (Themens et al., 2017, 2019), which is designed for high-latitude and Arctic (>50°) geomagnetic latitudes (Thayaparan et al., 2020). This model operates by performing numerical ray traces through a modelled background ionosphere and then introduces perturbations to the background E and F region to represent the dynamic electron density structures frequently observed in these regions. Thayaparan et al. (2020) provide a description of the effects of polar cap patches in the F-region ionosphere on OTHR operating in the high-latitude and Arctic region. This paper provides a similar analysis on the effects on E-region electron density structures known as sporadic-E, or Es.

Es is a localized layer of enhanced E-region ionization establishing an additional reflection layer that can alter HF radio wave propagation (Davies, 1990; Hargreaves, 1992; Kirkwood and Nilsson, 2000; MacDougall et al., 2000; Stocker and Warrington, 2011; Thayaparan and MacDougall, 2005). Es is typically observed at ~90–150 km altitude, and ranges from ~100 m to a few kilometres thick. Es lasts on the order of hours, and occurs sporadically. Horizontally, Es can be arbitrarily shaped depending on ionospheric conditions. While Es layers have been observed with horizontal extents ranging from 50 to 400 km, the exact extent is less certain due to the field-of-view limitations of the observing instruments (typically incoherent scatter radar). Simulations of metal ion transport suggest they can have horizontal extents of up to several 1000 km (Huba et al., 2019). The electron density can be high enough to cause the plasma frequency to exceed that of the F2 region with the observed critical frequency typically in the range of 4–10 MHz with values of up to 30 MHz possible (MacDougall et al., 2000; Thayaparan and MacDougall, 2005; Davies, 1990). Es layers are mainly composed of metallic ions originating from meteors that have then been compressed into thin layers by vertical wind shears and/or electric fields. Yue et al. (2016) provide an overall occurrence map of GNSS outages that they relate to auroral and Es structures in terms of magnetic latitude and magnetic local time based on a 5-year period of radio occultation signal amplitude observations and show Es occurrence has a two-cell pattern that peaks in the auroral zone at 00-06 MLT. They attribute this distribution to small-scale electric field variations in the nightside ionosphere. This description is consistent with the literature (e.g., Kirkwood and Nilsson, 2000), and is evidenced by the agreement between the polar electric potential contours determined by the Weimer05 model (Weimer, 2005) for average solar wind and interplanetary magnetic field conditions over the same interval (see Fig. 3 of Yue et al., 2016).

At high latitudes, Es takes on several characteristic forms including height-spread Es and thin Es. Height-spread Es is characterized by transient electron density enhancements over a range of altitudes. The electron density structure tends to be patchy such that the F-region is detectable. This phenomenon is most commonly observed during the late evening or midnight (local) hours with the occurrence maximum observed during the winter months (MacDougall et al., 2000). Thin Es, in contrast, is a narrow layer (≤5 km) and observed at the low end of the altitude range. Electron density tends to be intense, having a blanketing effect that blocks the F-region ionosphere from bottom-side observation. Thin Es is more frequently observed on the dayside and during the summer months due to the persistence of metallic layers caused by increased photoionization (Thayaparan and MacDougall, 2005; Kirkwood and Nilsson, 2000; MacDougall et al., 2000). Summer occurrence of height-spread Es is possible, but may be blocked due to the blanketing effect of thin Es (MacDougall et al., 2000).

Es can be an efficient radio wave reflector capable of altering radio wave propagation paths from those predicted by ray tracing models by supporting unexpected E-region reflections (e.g., FEF propagation, in which radio waves bounce between the F and E regions) (e.g., Davies, 1990; Lied 1967; Sherstyukov et al., 2009). For some frequencies the extra reflecting layer enhances the quality of the received signal by reducing the number of propagation paths through blanketing of the F-region. However, in some instances, multipath propagation introduced by the extra reflecting layer causes signal degradation (Sherstyukov et al., 2009). Es can also improve radio wave propagation by increasing the range of useable frequencies by raising the MUF. However, Es is not necessarily a reliable medium for improved radio wave propagation due to the unpredictable and transient nature of the phenomena which can lead to irregular or inconsistent signal strength.

This paper describes an initial investigation into the impacts of Es on HF radio wave propagation within the polar cap. This is accomplished through an event study in which an Es layer was clearly observed to facilitate consistent HF radio propagation at higher frequencies than normal over the Canadian Arctic for several hours. During this time, transmissions were received with a higher signal-to-noise ratio (SNR) than usual as well. These effects were modelled using HIPLAB to demonstrate the change in transmission paths for varying frequency. Section 2 describes the instrumentation and ray tracing model utilized in this paper. Section 3 presents the event, which is expanded on in Section 4 to begin a discussion on the overall implications of sporadic-E on HF radio wave propagation at high latitudes.

2. Instrumentation and ray tracing model

2.1. HF transmitter network

Natural Resources Canada (NRCan) operates a small HF network to study the effects of space weather on HF radio wave propagation (Cameron et al., 2021). 500 W transmitters with end-fed V antennas (https://www.bwantennas.com/acs.html) are located in Ottawa (OTT), Yellowknife (YKC), and Fort Churchill (FCC), and additional installations are planned for Resolute Bay and Iqaluit, see Fig. 1a. These are paired with a directional receiver (employing an array of elevated feed vertical monopoles) located in Alert (ALE). The selection of the transmitter sites allows the study of propagation paths that travel through the sub-auroral, auroral, and polar cap regions.

While this study does not use any data from the NRCan HF radio network, it does use HF radio propagation data sourced from the Qaanaaq (QAN), Greenland, to Alert (ALE) link of a defunct transmitter network operated by the University of Leicester, upon which the NRCan network is based (e.g., Warrington et al., 2016, 2017). The two networks share a radio receiver, and share similar transmission schedules. The QAN transmitter also employed an end-fed V antenna, though it was supplied with only 100 W of power. The QAN-ALE link is considered in this study due to its short distance and high latitude location, making it ideal for observing impacts from high-latitude sporadic-E without contamination from lower latitude phenomena (e.g., auroral absorption).

Each transmitter sends staggered Barker coded signals, at frequencies of 4.6, 7.0, 8.0, 10.4, 11.1, and 14.4 MHz, multiple times per hour. The receiver listens on a set schedule for the Barker coded sequences at the corresponding frequencies. If the correct sequence is detected, the receiver software records information about the received signal. If multiple signals are detected (e.g., from multiple propagation paths), the receiver software records information corresponding to all paths, but flags the signal with the highest signal strength. These flagged signals are analyzed to derive a number of parameters including, for example, time of flight (TOF), angle of arrival, and signal power.

2.2. Canadian Advanced Digital Ionosonde (CADI)

Sporadic-E is typically observed on an ionogram as a horizontal trace

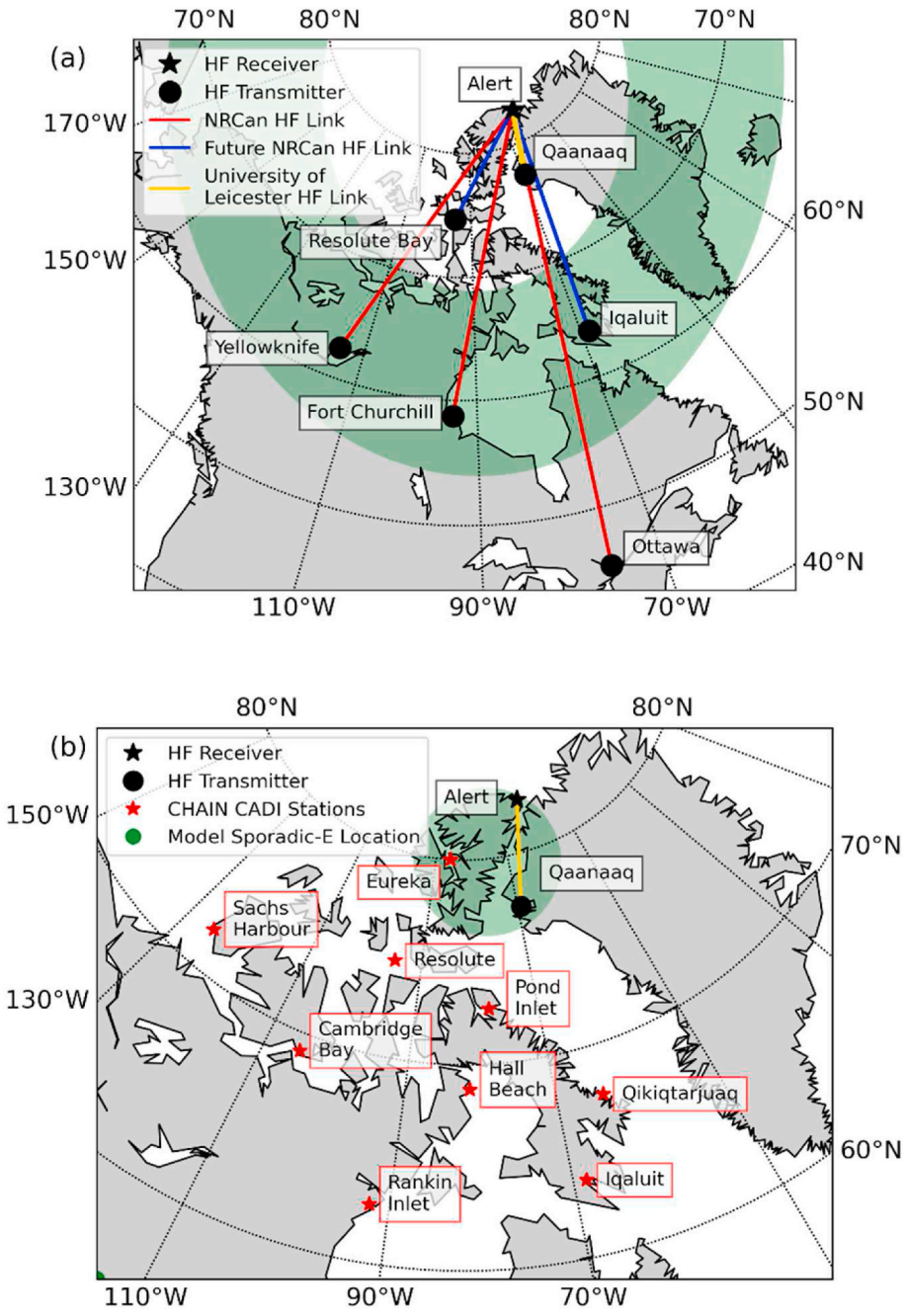

Fig. 1. (a) Map of the NRCan HF transmitter network. Red lines indicate currently running links, blue lines indicate future links, and the yellow line indicates a previous University of Leicester owned link. Green shading indicates the auroral zone region. (b) Map showing the locations of all CHAIN CADI instruments. Also included are an HF transmitter located at Qaanaaq, and an HF receiver located at Alert. Green shading indicates location of a model sporadic-E layer centered 200 km East of Eureka with a radius of 400 km.

of echoes at E-region altitudes extending to frequencies >5 MHz either as a thin line or a diffuse band in altitude a few tens of kilometres thick. Some examples of Sporadic-E in ionograms are seen in Fig. 2. Focusing on the 19:00 UT ionogram, the horizontal band of signal at ~100 km virtual height is indicative of a blanketing sporadic-E layer with a peak frequency of at least 10–11 MHz. The subsequent horizontal bands at 200 km, 300 km, and 400 km altitude are caused by multiple hops from the sporadic-E layer.

This study uses ionosonde data collected from the Canadian Advanced Digital Ionosonde (CADI) instruments of the Canadian High Arctic Ionospheric Network (CHAIN) (Jayachandran et al., 2009). Station locations are illustrated in Fig. 1b. Each CADI station is composed of a 4-antenna array of center-fed dipoles in a square (30-m length) configuration, with one receiver associated with each antenna, and produces one ionogram each minute at all sites except Eureka and Sachs Harbour, where they produce one ionogram every 5 min. In addition to ionograms, these ionosondes also measure plasma drift at 30-s time resolution using a fixed frequency mode (Jayachandran et al., 2009). The CADI located at Eureka, NU (EUA) with geographic coordinates of (79.99° N, 274.10° E) is considered in this study due to its close proximity to the QAN-ALE transmission path. All ionogram data, used in this study to measure sporadic-E intensity and height, were processed manually by an expert experienced with the CHAIN CADI systems.

This study also uses data from a Digisonde that operated in Qaanaaq (76.54°N, 291.56°E) during the time of the Es event. Data from this ionosonde were manually scaled by an experienced ionogram interpreter using the Global Ionospheric Radio Observatory's (GIRO) SAO Explorer tool [Reinisch and Galkin, 2011]. All Qaanaaq Digisonde data used in this study were acquired through the GIRO repository, accessible through SAO Explorer with further information available at http://giro.uml.edu/.

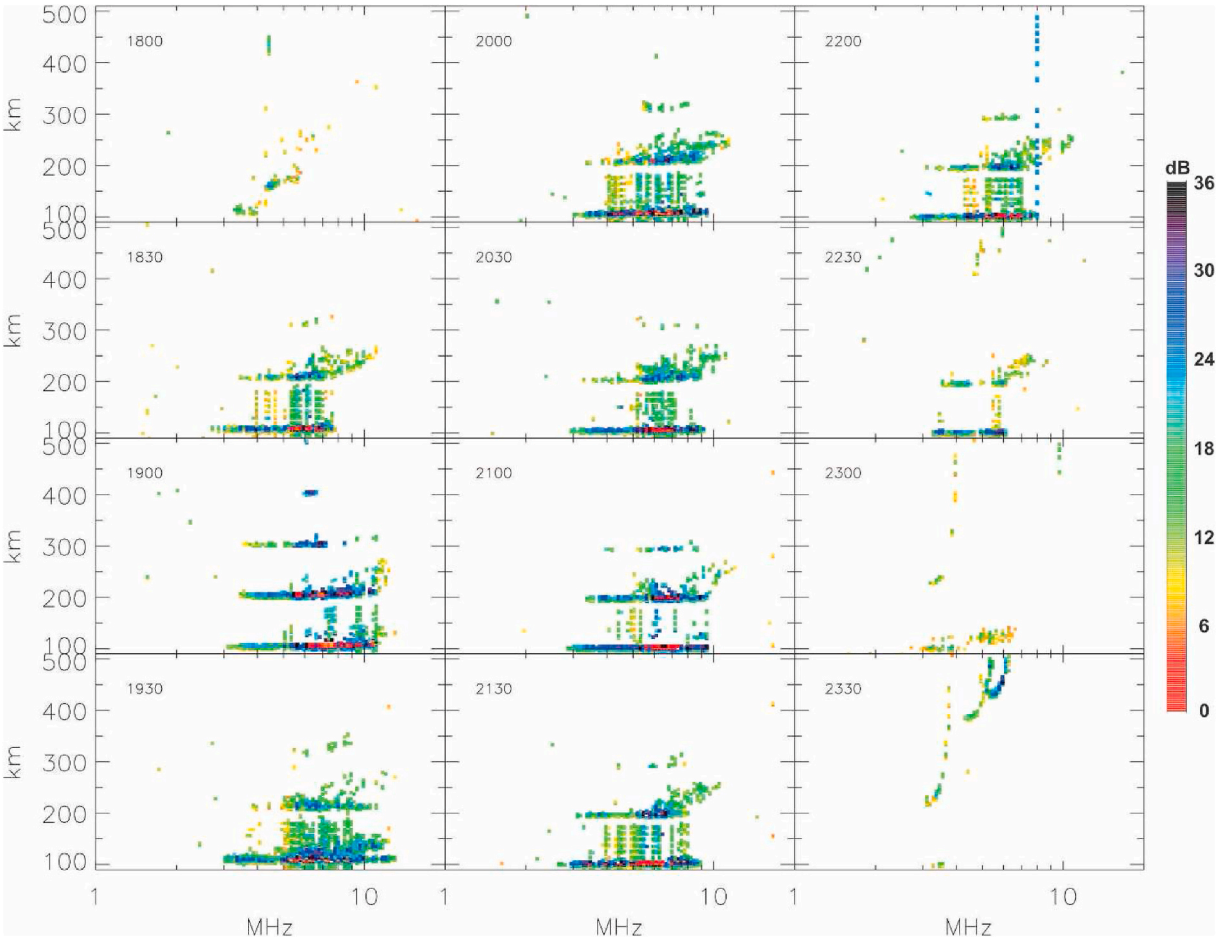

Fig. 2. CADI ionograms for 18:00 to 23:30 UT in 30-min intervals for July 11, 2012 for the Eureka station.

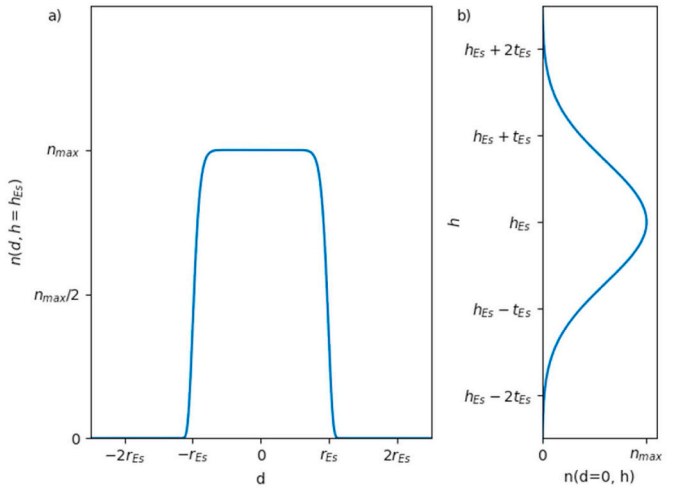

Fig. 3. (a) Horizontal profile of electron density at the sporadic-E height (h_{Es}), and (b) vertical profile of electron density at d = 0 for the model sporadic-E layer used in this study.

2.3. HF radio wave propagation model

OTHR surveillance is supported through a modelling technique called ray tracing which predicts high frequency (HF) radio wave propagation paths. Ray tracing uses numerical integration techniques to trace the paths of many radio waves through a model of the ionosphere, and it can be improved through the incorporation of real-time ionospheric measurements and models that represent ionospheric disturbances, such as sporadic-E or polar cap patches. This study uses the HIPLAB 3-D ray tracer toolbox. HIPLAB uses the ray tracer of Zaalov et al. (2003, 2005), and Warrington et al. (2012, 2016), a modified version of the Jones & Stephenson ray tracer (Jones and Stephenson, 1975), which traces HF radio waves by calculating the index of refraction in a model ionosphere using the Appleton-Hartree equations and then solving for the trajectory by numerically integrating the Hamiltonian ray path equations (Haselgrove, 1963). HIPLAB can incorporate models for high-latitude features found in the polar cap, auroral, and sub-auroral ionosphere including a mid-latitude trough, polar cap patches, and a sporadic-E layer.

In this study, the model ionosphere is generated in two steps: (1) a background ionosphere is generated, (2) model ionospheric disturbances are added in user specified locations. The background ionosphere employed in this paper is the Empirical Canadian High Arctic Ionospheric Model (E-CHAIM), which is an empirical model of ionospheric electron density in the high latitude (>50° geomagnetic latitude) region (Themens et al., 2017, 2018, 2019). E-CHAIM represents ionospheric density by a series of spherical cap harmonic expansions of various sub-models of ionospheric features. The parameters in these harmonic expansions are determined from millions of ionosonde and radio occultation measurements. E-CHAIM is able to reproduce diurnal, seasonal, solar cycle, and some degree of geomagnetic variability in electron density, making it a suitable model for exploring how different ionospheric conditions affect HF radio wave propagation. Throughout this paper E-CHAIM version 3.1.1 was used.

This study requires the addition of a model sporadic-E layer to the

background ionosphere. A single sporadic-E layer is modelled as a horizontal, circular, disk-shaped enhancement in electron density. For a sporadic-E layer with a vertical thickness t_{Es}, horizontal radius r_{Es}, and peak critical frequency $f_{c,\,Es}$, the electron density n as a function of distance from the center of the layer d at altitude h, is given by

$$n(d,h) = n_{\max} \exp\left(-\left(\left(\frac{d}{r_{Es}} \right)^2 \right)^8 \right) \exp\left(-\left(\frac{h - h_{Es}}{t_{Es}} \right)^2 \right) \quad (1)$$

and

$$n_{\max} = 1.24 \times 10^{10} \left(f_{c,Es}[\mathrm{MHz}] \right)^2 \mathrm{m}^{-3}. \quad (2)$$

Horizontally, the layer follows a Gaussian profile in which the content of the exponent has been taken to the power 8 (seen in the first exponent in Equation (1)), producing a profile with rounded edges and a flat-top. Vertically, the layer follows a typical Gaussian profile. Fig. 3 shows horizontal (a) and vertical (b) profiles of electron density given by the above model equations for sporadic-E. The background ionosphere and modelled Es layer are merged by applying the larger density of the two models at overlapping points, so that the spatial transition from sporadic-E to background ionosphere is as smooth as possible.

3. Event study: 10–12 July 2012

To demonstrate the impact of Es on HF radio wave propagation, we selected a period from 10–12 July 2012 in which enhanced HF propagation was observed from 16:50 to 21:35 UT July 11, 2012 along the QAN - ALE propagation path. The solar-terrestrial environment during this period is established to evaluate the likelihood of impacts to HF radio wave propagation from alternative sources. Fig. 4 shows relevant space weather conditions for the 10–12 July 2012 period. Solar wind and interplanetary magnetic field (IMF) parameters were evaluated based on data from the Advanced Composition Explorer (ACE) satellite data. For the 10–12 July 2012 period the IMF B_z varied between ±5 nT without any prolonged periods of negative IMF, and the solar wind speed slowly varied between 400 and 550 km/s. The AE index was somewhat elevated at ~500 nT prior to 09 UT on July 11, 2012, but dropped to <200 nT for roughly 12 h before rising to >500 nT until roughly 01 UT on July 12, 2012 where it once again dropped to <200 nT. The Dst index (not shown) was >-20 nT, without any major fluctuations.

Geostationary Operational Environmental Satellite (GOES) data were also examined to evaluate the solar X-ray flux and solar proton flux data for evidence of shortwave fadeout and polar cap absorption, respectively. The 0.1–0.8 nm GOES solar X-ray flux was observed to be $< 10^{-5}$ Wm^2 (<M-class flare) on July 11th, the date on which the Es layer was observed; the largest flares observed were of magnitude C9.9 and C5.6 peaking at 08:31 UT and 21:27 UT, respectively. There was an X1.4 flare that peaked at 16:49 UT on July 12th, hours after the Es event studied in this paper. During July 10th and 11th, the >10 MeV solar proton flux was <1 pfu, well below the 10 pfu threshold adopted to characterize a solar energetic particle event. There was a large increase in proton flux that occurred at 18:00 UT on July 12th, after the X1.4 solar flare, > 12 h after the Es layer had disappeared.

Across the three day interval 10–12 July 2012, NmF2 was gradually recovering from its depleted storm state due to geomagnetic activity that occurred on July 9, 2012. NmF2 returned to its normal state by the end of July 12th, as seen in Fig. 4g. The storm recovery also substantially modified the diurnal foF2 variation in the polar cap. Though the storm

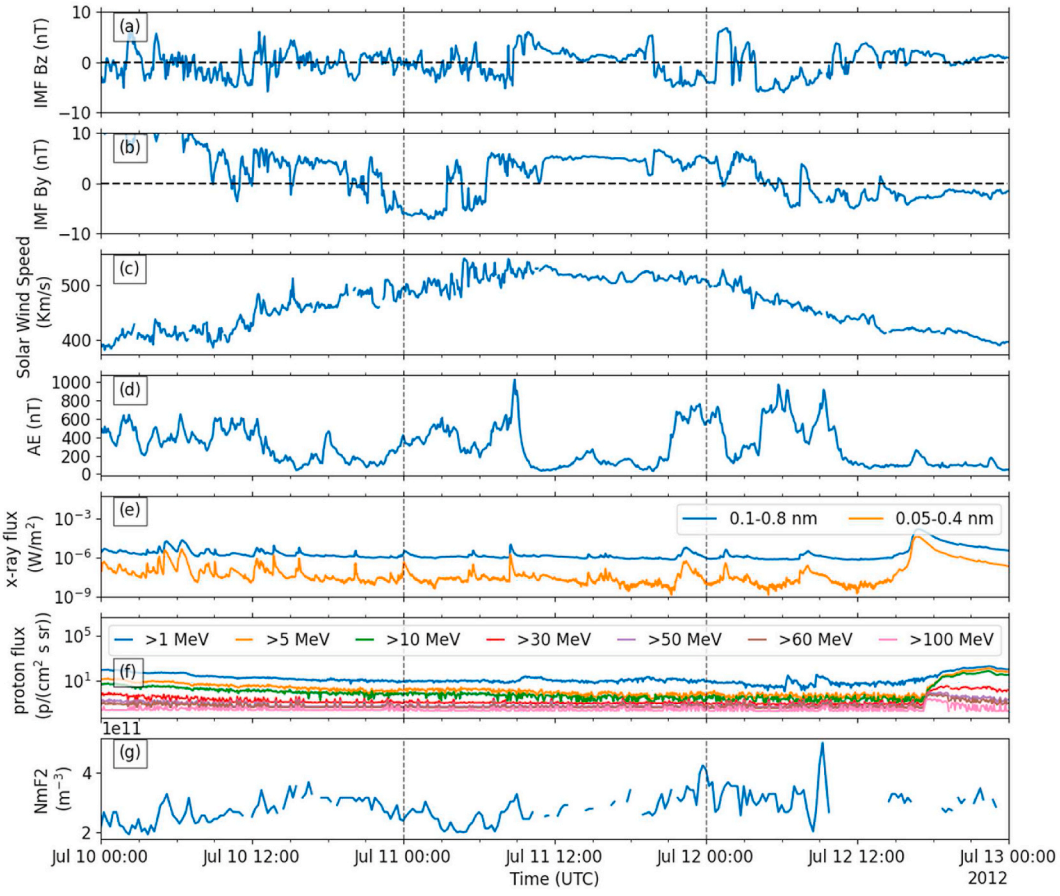

Fig. 4. (a) Interplanetary Magnetic Field Z-component (IMF Bz), (b) Interplanetary Magnetic Field Y-component (IMF By), (c) Solar wind flow speed, (d) AE index, (e) Solar X-ray flux, (f) Solar proton flux, (g) NmF2 over Qaanaaq from the Qaanaaq Digisonde for the 10–12 July 2012 interval.

recovery did result in a suppressed ionospheric critical frequency for part of the period, this effect can be separated from any enhanced propagation due to Es. Furthermore, based on the low activity demonstrated by the solar wind and IMF parameters, various geomagnetic activity indices, and the GOES solar X-ray flux and solar proton flux, it is unlikely that HF radio wave propagation was influenced by sources other than the Es and the storm recovery during the time the Es was present.

3.1. HF data for the QAN-ALE propagation path

Fig. 5 shows data measured by the Alert receiver on 10–11 July 2012 for the QAN-ALE propagation path. From the top down, panels show time series of the occurrence of signal reception, SNR, recorded time-of-flight (TOF), elevation angle of arrival, and azimuth angle of arrival. Frequencies plotted are: 4.6, 7.0, 8.0, 10.4, 11.1, and 14.4 MHz, which are each indicated by specific colors according to the legend.

Over the three-day window, signal reception and SNR illustrated in Fig. 4 change with time. On July 10, 2012, only the 4.6 MHz signal is detected steadily from 00:00–06:00 UT with an SNR of ~35 dB. Detection of the 8.0 MHz signal at an SNR of ~ -10 dB is intermittent during this period, likely due to the lower density of the nightside ionosphere which is not sufficient to reflect the higher frequency signals. After 06:00 UT, the three lower frequencies (4.6, 7.0, 8.0 MHz) start to be steadily detected at Alert. The SNR for 7.0 and 8.0 MHz rises from ~-10 to ~30 dB during this time, while the 4.6 MHz SNR lowers to ~20 dB. The three highest frequencies (10.4, 11.1, 14.4 MHz) are detected intermittently from 12:00–24:00 UT, with SNRs ranging from −10 to 30 dB, though the period of most consistent transmission is from ~13:30–19:00 UT. It will be shown in the following section that this period of enhanced transmission partially overlaps with a short-lived Es layer detected at Eureka and Qaanaaq.

Moving to July 11, 2012, until 10:30 UT, only the 4.6, 7.0, and 8.0 MHz signals are present in the data. At the start of the day, the 4.6 MHz SNR is ~35 dB, while the 7.0 and 8.0 MHz SNR is ~ -10 dB, having shifted from 30 dB over the last 2 h of the previous day. From 10:30–16:50 UT, the 10.4, 11.1, and 14.4 MHz signals start to be received at Alert intermittently. During this period, the lower three frequencies have an SNR of ~30 dB, while the upper three frequencies are at an SNR of ~ -10. Starting at 16:50 UT, all six frequencies are

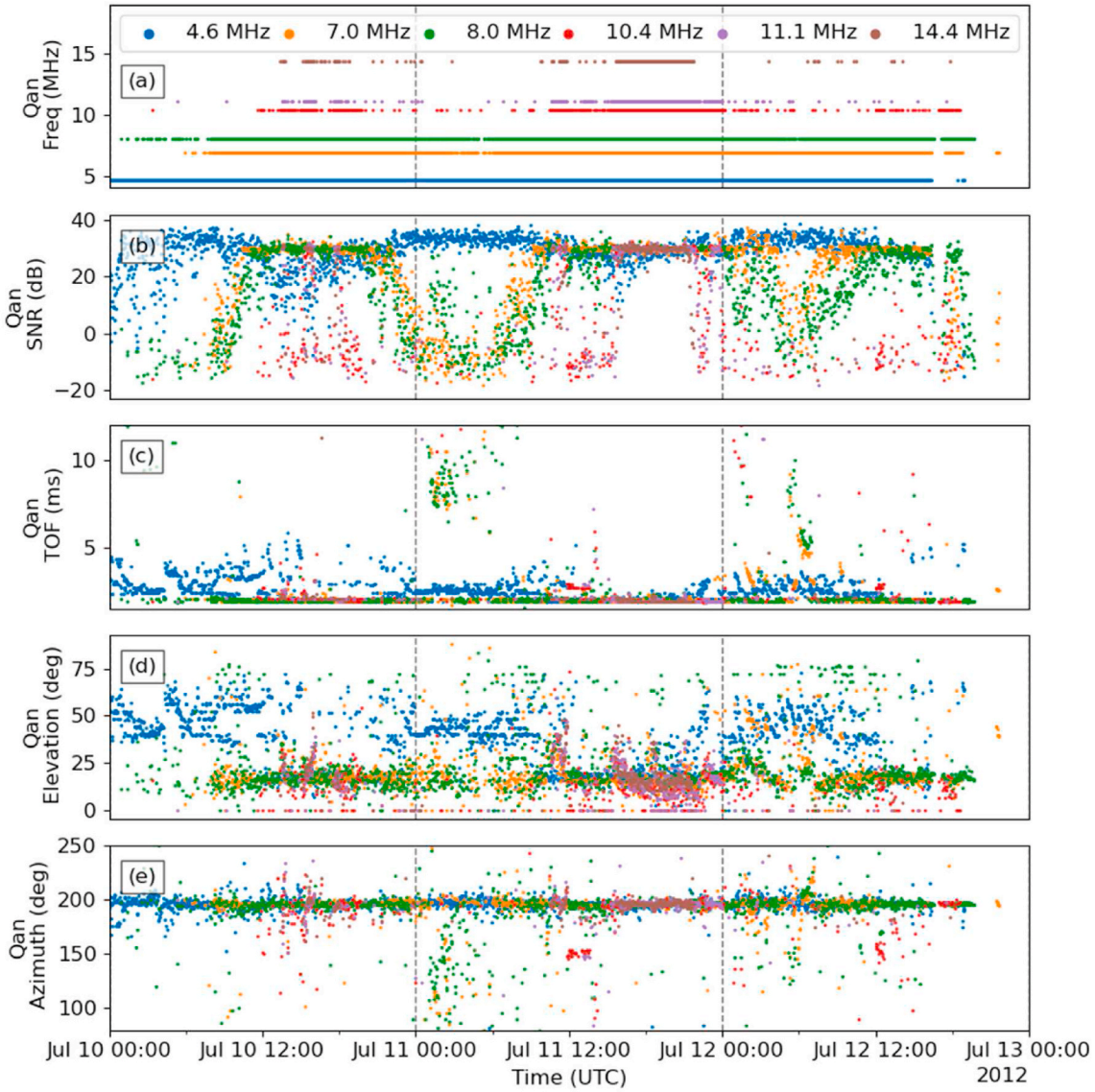

Fig. 5. (a) Periods of HF reception of signals at the prescribed frequency, (b) Signal to Noise Ratio (SNR), (c) Time of flight (TOF), (d) Elevation Angle, and (e) Azimuth Angle, for signals transmitted from QAN and received at ALE for the 10–12 July 2012 interval. Frequencies recorded are: 4.6 MHz (blue), 7.0 MHz (orange), 8.0 MHz (green), 10.4 MHz (red), 11.1 MHz (purple), 14.4 MHz (brown).

received at Alert steadily with ~30 dB SNR until 21:35 UT, when the 14.5 MHz signal drops out. The other five frequencies continue to be detected for the rest of the 11th, though with lowered SNR for 10.4 and 11.1 MHz. We show in the following section that this period of enhanced signal reception observed for 16:50–21:35 UT overlaps with a period in which a long-lived Es layer was detected at Eureka and Qaanaaq.

On July 12, 2012, the lower three frequencies are received at Alert steadily until 16:30 UT. The 4.6 MHz SNR is again slightly higher at ~35 dB, while the 7.0 and 8.0 MHz SNR drops from ~30 dB to ~ -5 dB, then rises back to 30 dB. Throughout the day the 10.4 and 11.1 MHz signals are received intermittently, occasionally joined by the 14.4 MHz signal, all with ~-10 dB SNR. Reception at 10.4 MHz becomes steadier after 12:00 UT, until all frequencies disappear in the last quarter of the day. This total dropout is likely due to a polar cap absorption event that started in the final hours of July 12, 2012 (See Fig. 3) caused by the enhanced solar proton flux.

Analysis of other signal parameters recorded by the HF receiver and plotted in Fig. 4 help clarify the propagation paths used to reach Alert over this three day period. On July 10, 2012, the 4.6 MHz TOF varies between 2 and 5 ms until ~14:30 UT, after which it drops to ~2 ms. The other frequencies (when present) generally have lower TOFs closer to 2 ms. Higher TOFs in general correspond to either paths involving more hops, reflections off higher ionospheric layers, or off-great circle propagation. Angle of arrival information can help untangle this. Based on simple spherical geometry, if the E and F regions are assumed to be at 100 and 250 km altitude respectively, then 1 and 2 hop E region propagation would result in ~18° and 34° received elevation angles respectively, and 1 and 2 hop F region propagation would result in 39° and 60° received elevation angles respectively. The elevation angle of the 4.6 MHz signal before 14:30 UT is ~40°, and the 7.0 and 8.0 MHz elevation angles are both ~15°. This suggests that at this time, based on the above listed angles, the 4.6 MHz signal reached Alert through some combination of 1 and 2 hop F-region reflection and 2 hop E-region reflection, while the 7.0 and 8.0 MHz signals reached Alert via 1 hop, E-region reflection. After 14:30 UT, the 4.6 MHz angle of arrival also drops to ~15°, indicating 1 hop E-region reflection. After ~21:00 UT, the 4.6 MHz TOF rises back to between 2 and 5 ms, and the elevation angle of arrival rises back to 40°.

TOF and elevation angle of arrival for the first half of July 11, 2012 is largely similar to that of July 10, 2012, although there is some noise in the TOF data on July 11, 2012 in the 7.0 and 8.0 MHz signals at 6–12.5 ms. TOF and elevation angle of arrival at 4.6 MHz are consistently higher than the same values for other frequencies (when present). Notably, during the period of enhanced signal reception (16:50–21:35 UT, July 11, 2012), TOF is low for all frequencies (~2 ms), and elevation angle of arrival is low as well (~15°). This is consistent with primarily single hop propagation off an Es layer at ~100 km altitude. TOF and elevation angle of arrival on July 12, 2012 again largely follows the pattern set on the 10th, until all signals drop out due to the polar cap absorption event at the end of the day.

Azimuthal angle of arrival over all six frequencies is largely constant over the three-day period plotted in Fig. 4, with an average angle of between 180° and 200° from N. This is consistent with great circle propagation from Qaanaaq to Alert, which has an azimuth of 196.79°. During the period of enhanced reception in the latter half of July 11, 2012, there is notably less fluctuation from the great circle direction. This is consistent with Stocker and Warrington (2011) who indicate that off-great circle propagation is predominantly observed for F-region propagation paths and is less often observed for E-region reflection. There is an interval between 01:00 and 06:00 UT on July 11, 2012 where azimuthal angle of arrival for 7.0 and 8.0 MHz fluctuates between 100° and 200°. At this time, the corresponding TOF is especially high, between 7 and 11 ms. The wide swing in azimuth, coupled with the high TOF points to a briefly stable off-great circle propagation path between Qaanaaq and Alert, possibly due to a convecting polar cap patch. While this period is not studied in this paper, off-great circle HF radio propagation is a topic of active research. For example, Thayaparan et al. (2021) presented simulations of off-great circle propagation due to polar cap patches in the context of OTHR operation. There is also a short period of 10.4 MHz signal being received at 150° azimuth. This signal has low SNR, and an associated TOF of 2.7 ms. The low TOF suggests that the propagation path was largely unchanged. Any deflection likely happened near Alert.

3.2. Ionosonde data

Fig. 2 shows ionograms for 18:00 UT to 23:30 UT at 30 min increments on July 11, 2012 from the Eureka (EUA) CADI instrument. The echo distribution indicates clear and strong reflection at ~100 km altitude, with an echo band of 15–20 km. This suggests an intense Es layer at ~100 km altitude persisting from 18:30 UT until 22:30 UT, with some growth and fading evident in the 30-min periods both before and after this interval. The layer is blanketing, with no clear F-layer visible until the 23:00 and 23:30 ionograms. Multiple (1, 2, and 3) hop reflecting layers are clearly visible, with the greatest signal strength at 19:00 UT where the critical frequency of the reflecting layer varied between from ~8 to 11 MHz. This time period overlaps with the period of high reception seen in Fig. 5 on 12–12 July 2012.

Fig. 6 presents time series data from both the Eureka CADI instrument (a-c), and from the Qaanaaq Digisonde (d-e). Fig. 6a shows the summed amplitudes at each ionogram virtual range over all frequencies measured at EUA for 10–12 July 2012. For the majority of the interval, echoes are observed at altitudes of >200 km, consistent with F-region reflections. From 16:45–18:00 UT July 10, 2012 there is evidence of a short-lived blanketing Es layer, characterized by a period of strong reflection at ~100 km altitude and a null in F-region echoes. The long-lived Es layer seen in Fig. 2, which may have caused the enhanced signal reception in Fig. 5, is observed beginning at 17:15 UT on July 11, 2012. It is characterized by a downward shift in echoes from roughly 150 km–120 km altitude over a 2-h interval, with an additional shift to ~100 km altitude from 18:00 UT to 23:00 UT and final termination of the Es layer at ~3:00UT on the July 12, 2012. Additional echoes are seen at this time at ~200 km and ~300 km altitude, representing 2 and 3 hop echoes. F-Region echo occurrence stops entirely during the later part of July 12, 2012, corresponding with the onset of a polar cap absorption event that began at 18:35 UT and peaked several hours later at 22:25 UT (see the solar proton event list maintained by NOAA SWPC at ftp://ftp.swpc.noaa.gov/pub/indices/SPE.txt).

Data from the EUA CADI were manually evaluated to determine the critical frequency and height of the Es layers present during the 10–12 July 2012 interval, see Fig. 6b and c. The short lived Es layer observed on July 10, 2012 from 16:45–18:00 UT is shown to have a critical frequency that rises from ~5.3 to 6.5 MHz over the event lifetime, at an average height of 103 km. Focusing on the longer lived Es layer, at 17:15 UT on July 11, 2012, critical frequency becomes elevated, quickly surpassing 5 MHz. Critical frequency varies over the layer's lifetime, rising to a maximum value of 13.0 MHz at 19:00 UT, before generally falling to 3.3 MHz at 03:15 UT, after which the layer disappears. Notably, there is a period from 23:30–00:15 UT in which the layer briefly is not observed. During the 17:15–03:15 UT interval, the height of the Es-layer generally decreases from ~150 km to ~95 km, where it remains for the duration of the Es layer.

Fig. 6d and e show Qaanaaq Digisonde measurements of Es layer critical frequency and height, respectively. Green shading in Fig. 5 (d) and (e) indicate times where Es was detected at Qaanaaq based on ionogram data (not shown). While the Qaanaaq Digisonde largely detects Es at times when Es was detected over Eureka, there are many other, short (~minutes) detections of Es over the entire interval not seen at Eureka. Although such short-lived events are not typically described, and are not described at length in this paper, Digisonde data does indicate these are blanketing layers that following the semi-diurnal tide signature of descent, consistent with Es. The lack of these structures at

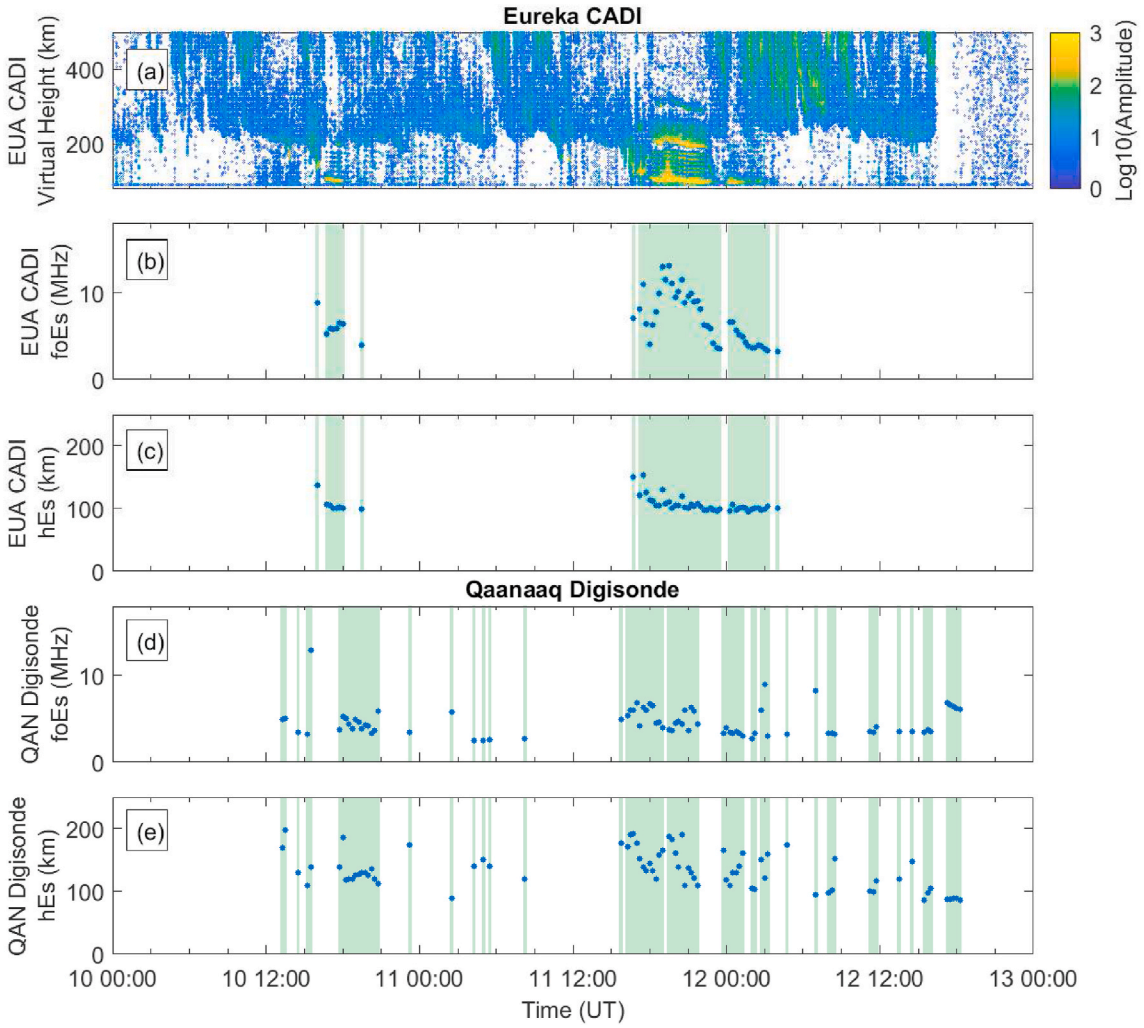

Fig. 6. (a) Summed amplitudes versus virtual height and time measured by the Eureka CADI for 10–12 July 2012. Es layer (b) critical frequency, and (c) height derived from Eureka CADI measurements as a function of time for the same time interval. Es layer (d) critical frequency and (e) height derived from Qaanaaq Digisonde measurements as a function of time. The green shading indicates time intervals for which the Es layer was detected by the ionosonde.

Eureka could possibly be due to differences in sensitivity between the two ionosondes, but is more likely that these layers are smaller and do not extend over the Eureka instrument. Overall, the data from the Qaanaaq Digisonde is much more variable than what was seen at Eureka. Both the critical frequency and detection altitude varies significantly over the 3 day interval. The average Es layer critical frequency measured at Qaanaaq is lower than what is measured at Eureka (averaging ~5 MHz). Altitude hEs varies from 100 to 200 km, with an average altitude of ~150 km, which is higher that the roughly steady 100 km reported at Eureka. Based on the ionogram data, the Es at Qaanaaq was generally thin. Variations in the layer height are attributed to gravity wave modulation of the layer convergence, which could induce turbulence resulting in height-spread Es at times. On July 10, 2012, the short lived Es layer detected at Eureka is also detected at Qaanaaq. It persists from 17:45–20:45 UT, longer than what was detected at Eureka, with a critical frequency that fluctuates between 3.3 and 5.9 MHz, and an altitude that varies between 112 and 185 km.

The long-lived Es layer detected at Eureka on 11–12 July 2012 is also detected at Qaanaaq from 16:15–03:15, with some short gaps in the middle of the interval. This layer has a critical frequency that varies between 2.7 and 9 MHz, at an altitude that varies between 103 and 191 km. After this layer breaks up, there are intermittent detections of Es not seen at Eureka.

The detection of a long-lived Es layer on 11–12 July 2012 at both Qaanaaq and Eureka suggests the enhanced propagation seen in Fig. 5 was due to the presence of a sporadic-E layer wide enough to be detected over both locations, and over at least part of the Qaanaaq-Alert propagation path. The distance between Qaanaaq and Eureka is ~450 km, likely suggesting an Es layer of >500 km diameter; larger than the 50–400 km observations cited above. Additionally, the differences in critical frequency and height between the two stations implies that the layer was not uniform. In the following section, we utilize both the Eureka and Qaanaaq ionosonde data to build simple Es models, which are then used in ray tracing simulations of 10–12 July 2012.

3.3. Modelled data

We performed two sets of ray tracing simulations of radio wave propagation at six frequencies (4.6, 7.0, 8.0, 10.4, 11.1, 14.4 MHz) along the QAN-ALE propagation path, over the 10–12 July 2012 time period. In each set of ray tracing simulations, a model sporadic-E layer was added to the model background ionosphere, as described in Section 2.3. The two sets of simulations only differed in the parameters used to define the sporadic-E layer model. For one, the critical frequency (f_{Es}) and height (h_{Es}) of the Es layer were set to vary with time according to the EUA CADI ionosonde measurements presented in Fig. 6b and c. For the other, the critical frequency and height of the Es layer varied with time according to the QAN Digisonde measurements seen in Fig. 6d and

e. Neither set of measurements perfectly captures the properties of the sporadic-E layer along the QAN-ALE propagation path. While the QAN Digisonde measurements capture the Es layer properties at the beginning of the path, the EUA measurements were taken closer to ALE. By performing ray tracing simulations using both sets of Es layer properties and comparing the two, we will gain a better overall understanding of how this Es layer affected HF radio wave propagation. What follows is a description of the procedure used to perform the ray traces.

Time steps were defined for 10–12 July 2012 at 15 min increments. For each time step, a background ionosphere was generated with E-CHAIM for that time, and supplemented with an Es layer at times when the critical frequency and height were non-zero, as seen in Fig. 6 (b) and (c), respectively. The 'storm' keyword was utilized in E-CHAIM in order to replicate the post-storm recovery conditions present at the time. The Es layer was modelled as a uniform 10-km vertically thick (t_{Es}) circular Es layer having a 400 km radius (r_{Es}) centered 200 km East of Eureka at (79.83° N, 75.71° W) geographic coordinates, using the Es model also described in Section 2.3. The size and position of the Es layer was chosen so that it overlapped with EUA, QAN, and the QAN-ALE great-circle path, which observed the effects of an Es layer. The modelled layer, the QAN – ALE propagation path, and EUA are illustrated in Fig. 1a. The critical frequency and height of the Es layer were set to vary with time for each set of ray tracing simulations as described above.

At each interval, rays were traced through the model ionosphere outwards from QAN in 0.2° increments of elevation from 0° to 90° and in increments of 0.4° azimuth for a 10° wide wedge centered on ALE. Rays landing within a 100 km radius of ALE were recorded for each time step. At any given time the rays corresponding to the highest signal power were used to calculate modelled parameters including TOF and elevation and azimuth of arrival, similar to the processing performed on the measured HF data. While the Qaanaaq transmitter was supplied 100 W during operation, power losses inherent to the transmitter antenna design meant that a smaller signal power was actually output by the antenna. Additionally, further signal power losses were known to occur at the receiver as well. To account for these two sources of loss, the simulated transmitter power was set to 6.25 W, based on previous investigation of this transmitter-receiver link. The transmitter and receiver were both modelled as simple vertical monopoles. While the actual transmitter and receiver were not actually simple vertical monopoles, the gain patterns are similar enough that any resultant errors are smaller than other possible sources of error (such as uncertainties in the amount of D-region absorption, or in previously mentioned losses in the transmitter and receiver). Solar absorption was applied to each ray before signal power was calculated. Some space weather contributions to absorption can be modelled with the D-region absorption prediction (D-RAP) model. This model accounts for D-region absorption due to solar X-ray flux and solar energetic proton flux, and is run by the NOAA Space Weather Prediction Center (https://www.swpc.noaa.gov/content/global-d-region-absorption-prediction-documentation). We compared the results of the ray tracing run with and without D-RAP absorption predictions applied, and found that the only appreciable absorption occurred during the first half of July 10, 2012, and the end of July 12, 2012. Neither of these times coincided with the Es studied in this paper. To simplify the description and analysis, we have omitted D-RAP absorption from the ray tracing results shown below.

Signal power was calculated by assigning a signal power to each ray based on the transmitter power, transmitter and receiver antenna gains, D-region absorption, and the geometry of the ray distribution over the surface area of a sphere surrounding the transmit antenna. The signal power for every ray that reached the target was then summed together, resulting in the received signal power. SNR was then computed by comparing the received signal power to the estimated noise floor. This noise floor was calculated based on the International Telecommunication Union (ITU) recommendation on radio noise (ITU-R P.372-15, 2021).

All ray traces in this study were performed assuming ordinary (O) mode propagation. We performed additional ray traces for the entire event assuming extraordinary (X) mode propagation as a check (not shown). While there were differences in the resultant X mode propagation paths, propagation during times when the Es layer was present was unchanged.

Fig. 7 plots the results of ray tracing simulations in which the Es model was based on EUA CADI measurements. The same parameters are plotted as those seen in the measured HF radio propagation data (Fig. 5). On July 10, 2012, transmission is limited to the 4.6 MHz signal, until 13:30 UT, when it is joined by the 7.0 MHz signal. At 16:00, signals at 8.0, 10.4, 11.1, and 14.4 MHz appear in the data, due to the short lived model Es layer placed above the propagation path. The enhanced propagation lasts only until 18:00 UT, when all frequencies above 7.0 MHz stop arriving at Alert. At 19:30 UT, 11.1, 10.4, and 8.0 MHz reappear very briefly, before all frequencies other than 4.6 MHz drop out for the day.

On July 11, 2012, signal reception is very similar to 10 July until the long-lived Es layer appears. Only 4.6 MHz signals arrive at Alert until 13:45 UT, when the 7.0 MHz signals begin to arrive. While the long-lived Es layer is modelled over the QAN-ALE propagation path beginning at 16:45 UT, all 6 frequencies are received at Alert. This enhanced reception persists until July 12, 2012 at 04:00 UT. The 14.4, 11.1, and 10.4 MHz signals drop out before the end of the interval, likely due to the decrease in the Es critical frequency in the hours before the Es layer disappears completely. There is also a brief dropout for all frequencies above 4.6 MHz from 23:15–00:15 UT, which lines up with the brief disappearance of the Es layer seen in Fig. 6. Transmission for the rest of July 12, 2012 is similar to the 10th and 11th, but without the effect of any more Es layers. 7.0 Mhz is detected from 13:45–19:45 UT, and 8.0 MHz is detected from 16:30–17:30 UT. The 4.6 MHz is detected for the entire day. The signal dropout seen at the end of July 12, 2012 in the measured HF data is not seen here, as the effects of the enhanced solar proton flux, and subsequent polar cap absorption, were not modelled.

Signal power for detected frequencies reaching Alert changes throughout the three-day period. On July 10, 2012, 4.6 MHz SNR varies quasi-sinusoidally between 12 and 30 dB, following diurnal ionospheric variation, likely due to changing D-region absorption. When present, 7.0 MHz SNR varies between 5 and 12 dB. All SNR change dramatically when the short-lived Es layer is present. The 4.6 MHz drops to −14 dB, while higher frequencies have successively higher SNRs between 12 and 41 dB. SNR variation on July 11, 2012 is very similar to the 10th, until the Es layer appears. The 4.6 MHs SNR drops again to −15 dB, and other frequency SNRs are spread out between 13 and 41 dB, with higher frequencies having higher SNR. After the Es layer is gone on July 12, 2012, the 4.6 MHz SNR follows the same sinusoidal pattern, 7.0 MHz SNR rises to 24 dB when present, and 8.0 MHz SNR briefly appears with 9 dB.

TOF and elevation angle of arrival over the three day interval largely transitions between two modes: ~2.4 ms TOF with ~40° elevation, and ~1.8 ms TOF with ~20° elevation. The 4.6 MHz signal is generally at ~2.4 ms TOF and ~40° elevation, and transitions to ~1.8 ms TOF and ~20° elevation when the Es layers are present on 10 and July 11, 2012. The 7.0 MHz and 8.0 MHz signals are generally received at ~1.8 ms TOF and ~20° elevation when detected at Alert, regardless of the presence of the Es layer, except for a brief period on July 12, 2012 from 16:30–17:30 when the 7.0 and 8.0 MHz TOF rises to 2.8 ms. The TOF and elevation modes seen here correspond to 1 hop propagation. While >1 hop paths did reach Alert, their associated signal power was lower than the 1 hop propagation. The change in TOF and elevation angle when the Es layers are present is due to the lower reflection altitude at these times. Azimuthal angle of arrival variation is minimal over the modelled three-day period. In general, it varies between 180° and 210°, in line with the on-great circle direction to Qaanaaq from Alert (196.79°).

The ray traced HF radio data in Fig. 7 can be compared to the observed HF radio data in Fig. 5. While there are clearly major differences between the measured and modelled data, the effect of the Es layer on propagation is similar. Setting aside periods in which Es was present,

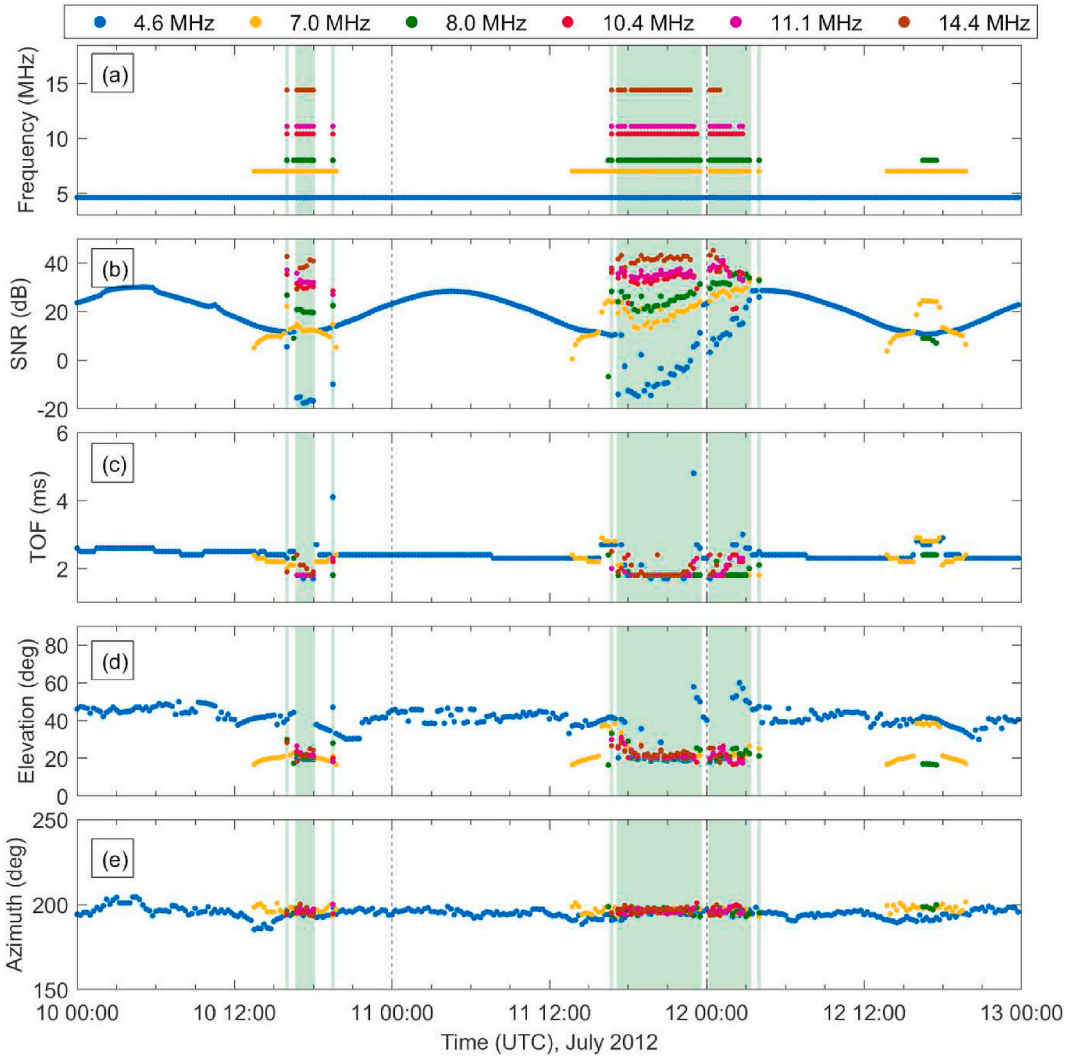

Fig. 7. Ray traced model data replicating the event shown in Fig. 5 for 10–12 July 2012 using Eureka CADI data. The model ionosphere was generated using E-CHAIM v3.1.1 with the addition of a sporadic-E layer, as described in the text. From the top, plotted quantities are: (a) Periods of HF reception of signals at the prescribed frequency, (b) Signal-to-noise ratio (SNR) (dB), (c) Time of flight (TOF) (ms), (d) Elevation (°), and (e) Azimuth (°). Frequencies recorded are: 4.6 MHz (blue), 7.0 MHz (orange), 8.0 MHz (green), 10.4 MHz (red), 11.1 MHz (purple), 14.4 MHz (brown). Green shaded regions indicate times sporadic-E was detected by the Eureka CADI instrument. Time is indicated by day of month and HH:MM on the bottom x axis, with the month and year indicated in the lower right.

signal reception in the measured data is generally better than in the modelled data. This means that higher frequencies are detected more often, and appear earlier in the day in measured data when compared to the ray traced data. For example, 7.0 and 8.0 MHz are present for the majority of time in the measured data, but are only present near local noon, and when aided by Es in the ray traced data. This could mean the background ionosphere provided by E-CHAIM underestimates electron density along the path for this time period (10–12 July 2012). Fig. 9 compares foF2 as measured by the Qaanaaq Digisonde to foF2 provided by E-CHAIM at Qaanaaq for 10–12 July 2012. The two curves follow approximately the same pattern, and at most differ by less than 0.5 MHz (apart from brief spikes). This suggests that any underestimation of electron density by E-CHAIM is occurring north of Qaanaaq.

SNR for all frequencies in the ray traced data shows much less spread than the measured data. However, during times with no Es, the range of variation for the two is fairly similar, with 4.6 SNR ranging between ~15 and 35 dB in both the measured and ray traced data. During times with Es though, the ray traced SNR exhibits much more stratification with frequency when compared to the measured SNR. TOF and elevation vary over similar ranges in the two figures, suggesting that the ray tracer is producing similar raypaths to what the real radio waves followed. Both the measured and ray traced azimuthal angle of arrival data are tightly clustered around the great circle direction from Qaanaaq to Alert (other than the brief interval on July 11th in the measured data).

Fig. 8 presents results in which the model Es parameters were determined by the Qaanaaq Digisonde measurements. As expected, at times when no Es layer is present, all reported quantities are essentially identical to those seen in Fig. 7, since the propagation conditions for ray tracing were identical at these times. During the times the Qaanaaq Digisonde reported Es, the ray tracing derived quantities are different from what was seen in Fig. 7. Overall, the more frequent detections of Es at Qaanaaq has resulted in more overall scatter in the data, as intermittent Es modifies propagation for a single time interval before disappearing. The more variable, and overall lower Es critical frequency results in less overall propagation at high frequencies. For example, in Fig. 7a, the 14.4 MHz signal was detected almost the entire time the long-lived Es layer was present, from July 11, 2012 16:45 UT – July 12, 2012 04:00 UT. In Fig. 8a, during the same time interval, the 14.4 MHz signal was only detected intermittently. This difference is also present for the shorter lived Es layer seen on July 10, 2012. Of the two Es models, the EUA informed model seems to better replicate the data seen in Fig. 5.

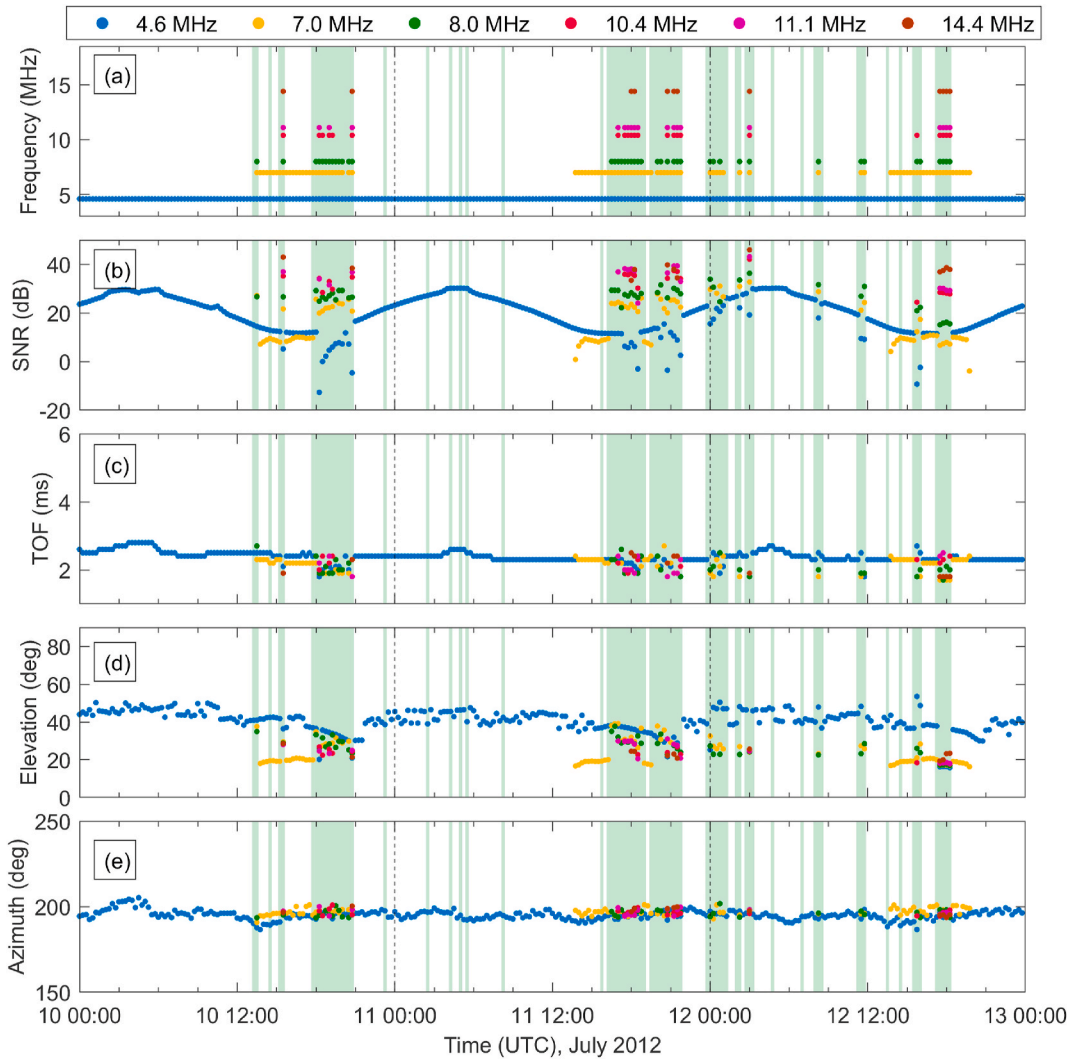

Fig. 8. Ray traced model data replicating the event shown in Fig. 5 for 10–12 July 2012 using Qaanaaq Digisonde data. The model ionosphere was generated using E-CHAIM v3.1.1 with the addition of a sporadic-E layer, as described in the text. From the top, plotted quantities are: (a) Periods of HF reception of signals at the prescribed frequency, (b) Signal-to-noise ratio (SNR) (dB), (c) Time of flight (TOF) (ms), (d) Elevation (°), and (e) Azimuth (°). Frequencies recorded are: 4.6 MHz (blue), 7.0 MHz (orange), 8.0 MHz (green), 10.4 MHz (red), 11.1 MHz (purple), 14.4 MHz (brown). Green shaded regions indicate times sporadic-E was detected by the Qaanaaq digisonde instrument. Time is indicated by day of month and HH:MM on the bottom x axis, with the month and year indicated in the lower right.

One other notable difference in periods of HF reception can be seen at the end of July 12, 2012. The Qaanaaq Digisonde detected Es at ~18:00 UT, resulting in enhanced reception at this time in the ray trace results. This enhanced reception was not seen in the EUA Es model results (since EUA did not detect any Es), or in the measured data. The lack of any enhanced Es in the measured HF radio data is likely due to the polar cap absorption event that occurred on July 12, 2012.

Other calculated parameters also show differences when compared to Fig. 7. Unlike Fig. 7b, the 4.6 MHz SNR does not drop nearly as much during times Es is present. Other frequencies show noticeable differences in SNR as well. The 7.0 and 8.0 MHz SNR is higher by ~5 dB. SNR for the upper three frequencies are lower by ~5 dB in some cases, and close to the same in others. Due to the overall higher Es altitude as measured at EUA, the ray traced TOF during times Es is present does not drop as much as it does in Fig. 7c. This is not surprising, since a higher Es layer would mean a longer propagation path. This same effect is seen in the EUA ray traced elevation (Fig. 8d), in which the higher Es layer means higher received elevation angles when compared to Fig. 7d. When comparing TOF and elevation to the measured HF radio data, the spread in the measured HF data makes it difficult to judge which model is more accurate than the other. Unsurprisingly, there is very little difference in the received azimuth. In both ray tracing simulations, propagation is entirely on-great circle.

In general, during times when Es is present, signal parameters using both models change in similar ways to real data. All six frequencies arrive at Alert more often when the model or real Es is present, due to the relatively high Es critical frequency. TOF and elevation angle both decrease, due to the lower altitude of the reflecting Es layer than the F2 layer. The only signal parameter that behaves differently in simulations when compared to the measured data is SNR. In the measured data, the Es layer causes the SNR to tightly cluster around 30 dB for all frequencies. When Es is present in the ray traced data, as mentioned above, SNR is much more stratified, ranging from ~-20 to ~40 dB. While there are discrepancies in the SNR comparison, the rest of the parameter comparisons point to this simple Es model being able to replicate the change in propagation paths seen in the measured HF radio data.

4. Implications of sporadic-E on HF radio wave propagation

As demonstrated by the series of sporadic-E events that occurred from July 10–12 2012 presented in this paper, a sporadic-E layer has the potential to strongly impact HF radio wave propagation. Sporadic-E

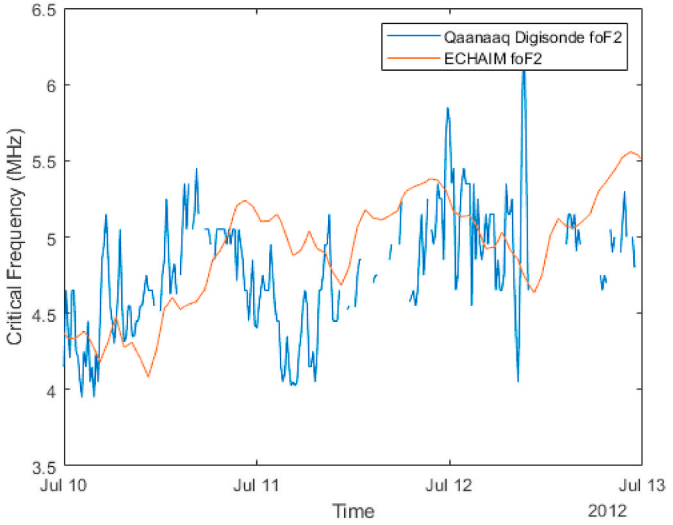

Fig. 9. Qaanaaq Digisonde and E-CHAIM foF2 at Qaanaaq plotted from 10–12 July 2012.

layers are vertically thin and flat, and therefore tend to improve HF radio propagation range and received signal power without disrupting the signal. This was demonstrated by these events as a focusing of the SNR at 30 dB and a complete loss of noise during the period where a sporadic-E layer was observed. Additionally, the measured HF radio data presented in Fig. 5 supported the results of Stocker and Warrington (2011) that sporadic-E layers do not refract radio waves in off-great-circle directions. None of the sporadic-E layers detected by either the Qaanaaq Digisonde or the Eureka CADI resulted in appreciable off-great circle propagation as measured by the Alert HF radio receiver. It is not surprising that the ray traced data showed no off-great circle propagation either, since the model Es layer was placed directly above the propagation path. Any theoretical off great circle propagation due to sporadic-E would have to be the result of interaction with the edges of the thin layer.

4.1. Generalized effect of Sporadic-E on HF radio wave propagation

The effect of the strong reflecting surface provided by sporadic-E is to change the reflection altitude and critical frequency, in some cases allowing for signal propagation to locations not otherwise accessible via HF radio wave propagation. Fig. 10 illustrates the effect of sporadic-E on HF radio wave propagation with vertical plots of ray trajectories for one time slice of the Es event studied in the previous section. In the upper panel 5 MHz rays are propagated through an E-CHAIM generated ionosphere for 20:00 UT July 11, 2012. Rays are transmitted toward Alert from Qaanaaq at elevations angles ranging from 3° to 90° in 0.5° increments. Trajectories of all traced rays that landed on the ground are plotted on top of a map of vertical electron density along the great circle path from Qaanaaq to Alert. Rays with a sufficiently low initial elevation angle are refracted by the higher electron density in the F-region (~275 km altitude) back toward the Earth, overshooting Alert, resulting in signal reception >1000 km from Qaanaaq (not shown in the plot).

In the lower panel of Fig. 10, the same background ionosphere is supplemented by the model sporadic-E layer seen in the EUA CADI data for this time, and studied in the above event study. The sporadic-E layer parameters used were $f_{Es} = 9.44$ MHz, $h = 105.15$ km, $t_{Es} = 10.0$ km, $r_{Es} = 400$ km. Only rays that landed within 50 km of Alert are plotted, for clarity. Compared with the upper panel, the sporadic-E layer refracts rays with higher initial elevation angles back toward the Earth. The lower altitude of the layer results in signal reception at Alert from 1 hop, 2 hop, and 3 hop propagation paths (rays were only tracked for up to three hops).

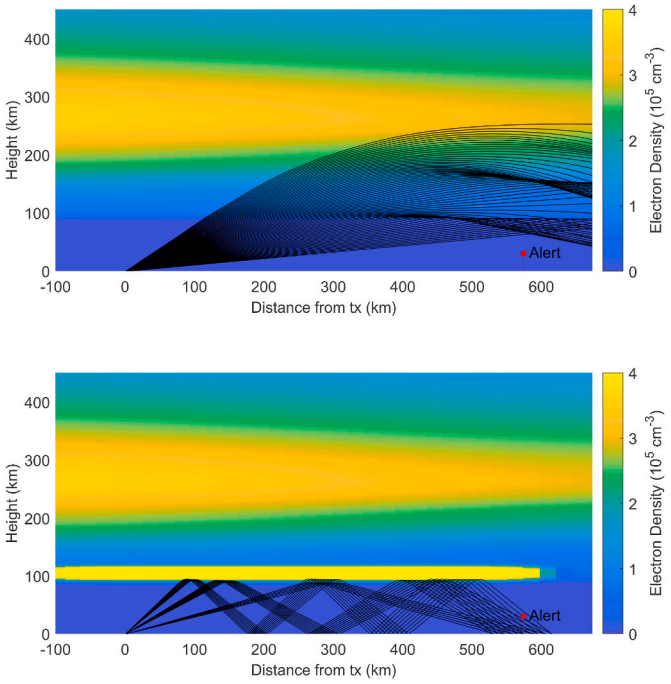

Fig. 10. Comparison of 5 MHz vertical ray trajectories through an E-CHAIM v3.1.1 model ionosphere generated for 20:00 UT July 11, 2012 without (top) and with (bottom) the model disk shaped sporadic-E layer. Model parameters for the Es layer were taken from CADI measurements of the Es layer at this time ($f_{Es} = 9.44$ MHz, $h = 105.15$ km), and the physical dimensions were the same as the model used in the previous section ($t_{Es} = 10.0$ km, $r_{Es} = 400$ km). In order to properly see the background ionospheric density, the color scale was set to a maximum of 4×10^5 cm^{-3}, though this saturates the Es layer, which has a peak electron density of 1.14×10^6 cm^{-3}. In the bottom panel, only rays that landed within 50 km of Alert are plotted.

4.2. Impact of Sporadic-E on available frequencies and elevation angles

To gain a better understanding of the impact of a sporadic-E layer on HF radio wave propagation consider the impact across the entire range of frequency and elevation angles by considering signal power. Fig. 11a shows signal power in terms of frequency and transmitted elevation angle generated from a series of ray tracing runs through an E-CHAIM v3.1.1 model ionosphere for July 11, 2012 at 20:00 UT. Signal power is estimated for a 500 W transmitter in Qaanaaq being received in Alert based on a series of ray traces at frequencies ranging from 3 to 18 MHz in 0.2 MHz increments. Rays were traced in elevation increments of 0.2° from 0° to 90°, and in azimuth increments of 0.5°, in a 4° wide azimuthal range centered on the target direction. Signal power was calculated assuming a vertical monopole gain pattern with solar absorption (no space weather contributions) applied to the ray trace. Three clear signal bands can be seen in the image, corresponding to 1 hop (elevation <30°), 2 hop (elevation 30°–60°), and 3 hop propagation (elevation >60°). No signal propagation is seen above 6.6 MHz, due to the relatively low ionospheric electron density.

Fig. 11b was generated using the same parameters used to generate Fig. 11a, but with the addition of the sporadic-E layer modelled in Figs. 7 and 8 in Section 2.3. At this time, the sporadic-E layer was at an altitude of 105.15 km, and the critical frequency was 9.44 MHz according to the EUA CADI data. Similar to Fig. 11a, three propagation paths are present. However, each are observed at much higher frequencies than the 6.6 MHz maximum observed in Fig. 11a. One-hop propagation persists up to 26.2 MHz, 2-hop propagation reaches 15.4 MHz, and 3-hop propagation reaches 12.2 MHz. All three paths involve propagation via reflection off the added sporadic-E layer. The higher critical frequency of the sporadic-E layer allows for much higher frequency reflection, especially

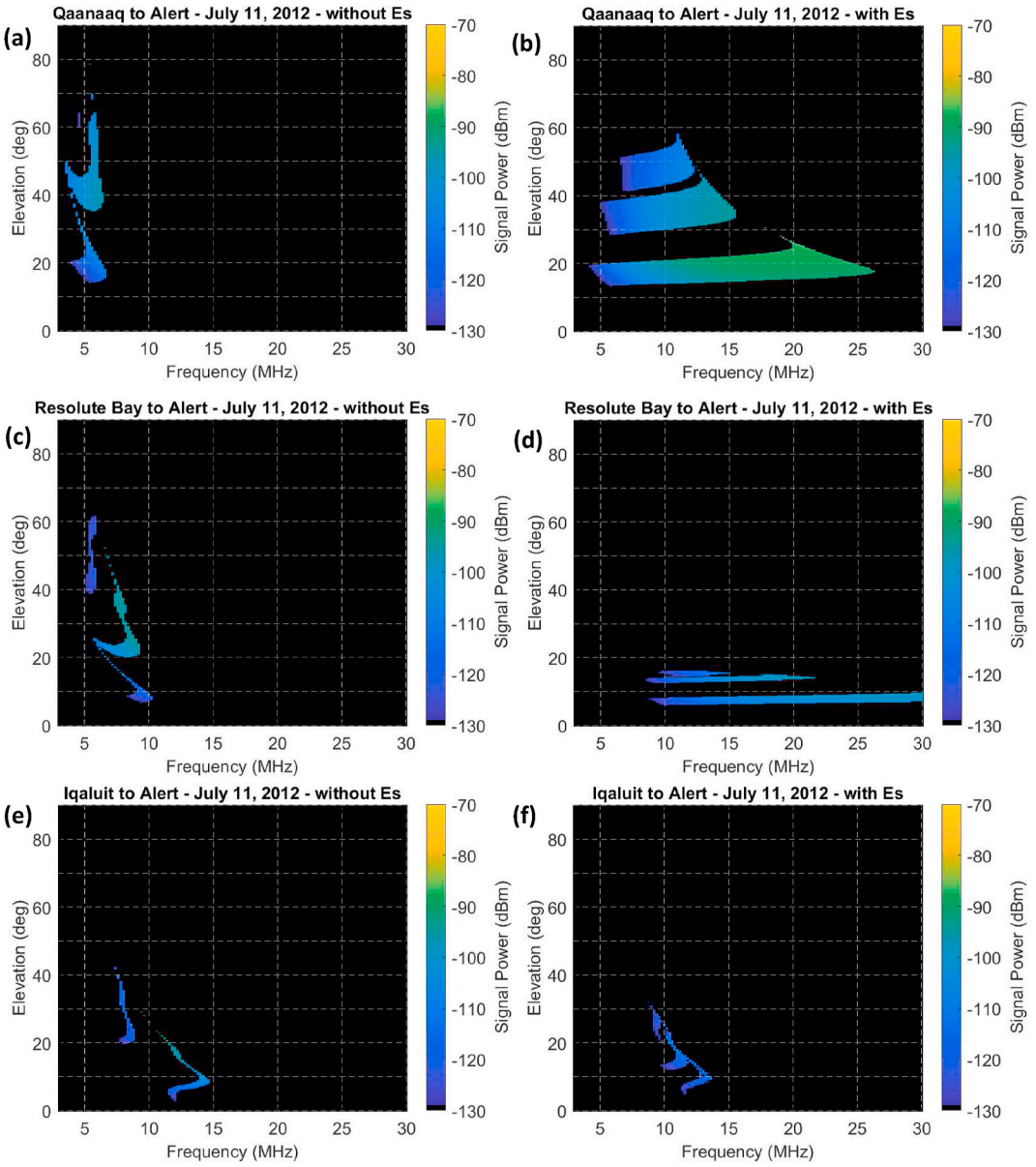

Fig. 11. Ray traced signal power versus frequency and elevation detected by a receiver in Alert, Nunavut, through a model ionosphere generated by E-CHAIM (v3.1.1) for 22:00 UT July 11, 2012, for the following setups: (a) A transmitter in Qaanaaq (~574 km away), (b) a transmitter in Qaanaaq with an added sporadic-E layer, (c) a transmitter in Resolute Bay (~1092 km away), (d) a transmitter in Resolute Bay with an added sporadic-E layer, (e) a transmitter in Iqaluit (~2092 km away), (f) a transmitter in Iqaluit with an added sporadic-E layer. The thickness of some traces are due to the radius (100 km) of the collecting area used. In all cases, the transmitter operating power was set to 500 W, and the transmitter and receiver gain profiles were set to be a simple vertical monopole. The sporadic-E layer characteristics were the same as used in the case study presented in Section 3 for 22:00 UT on July 11, 2012.

when the waves reach the ionosphere at an angle. There is also a clear shift to lower elevation angles for the 2 and 3 hop propagation paths. This is due to a change in reflection height from the F region (~200–400 km) to the sporadic-E layer (105.15 km). To reach the same target, a lower reflection height necessitates a lower elevation angle. The elevation required for 1-hop propagation does not change because 1-hop propagation was already occurring via the E-region for the lowest frequencies, even in the absence of a strong Es layer.

Sporadic-E is expected to impact longer propagation paths differently than shorter paths. Consider, for example, propagation from Resolute Bay to Alert (RES - ALE), representing a longer great circle path length of 1092 km. Fig. 11c and d show ray traced signal power vs frequency and elevation for propagation through the same ionospheres as Fig. 11a and b, from RES to ALE. Propagation in the absence of the sporadic-E layer (Fig. 11c) is limited to frequencies between 5 and 10.3 MHz, at a range of elevations reaching up to 62°. Similar to QAN-ALE, three propagation paths are present. The addition of the Es layer over Qaanaaq (Fig. 11d) improves propagation at higher frequencies, but impedes propagation at lower ones. Signal reception is seen at frequencies from 9 to 40 MHz via three distinct propagation paths. The full frequency range is not shown in Fig. 11d, but was confirmed with additional ray traces. Unlike the QAN-ALE path, these paths all have initial elevations <16°. This is due to the longer distance from transmitter to target. For a ray to reflect off the bottom of the Es layer at a longer distance, it needs to have an even lower initial elevation angle. The reduction of lower frequency propagation is something that was not seen for QAN-ALE. In Fig. 11c, the lower frequency propagation occurred for high initial elevation angle rays. With the added sporadic-E layer in Fig. 11d only covering the latter part of the propagation path, these low frequency – high elevation rays reflected off the F layer, and

then subsequently reflected upwards off the top of the Es layer into space, never reaching the target. One might wonder why the low elevation angle bands seen in Fig. 11d also aren't present at frequencies lower than 9 MHz either. This is because the low frequency, low elevation angle rays experience too much absorption to be detected (received signal power is < -130 dBm), even though they do reach the target. The increased absorption is due to a combination of the low frequency rays experiencing more absorption, as well as the low elevation angles causing the rays to spend more time in the D-region, also leading to more absorption.

Fig. 11e and f show signal power vs frequency and elevation for propagation from Iqaluit to Alert (IQA-ALE), with a great circle distance of 2092 km. These two panels show propagation though ionospheres following the same pattern as Fig. 11a/c and 11 b/d. In Fig. 11e, propagation in the absence of the Es layer is more limited than in Fig. 11a and c. There is a band of propagation from 7.5 to 8.8 MHz, and another from 10.5 to 14.6 MHz. These propagation paths exist over a much more narrow range of frequencies and elevations, due to the much longer distance between IQA and ALE. The addition of the Es layer over Qaanaaq actually reduces the available frequencies for propagation to Alert, as seen in Fig. 11f. The maximum signal power is reduced as well. Due to the long distance between Iqaluit and Alert, the low altitude Es layer acts more as an obstacle for the rays than a propagation aid. Rays with elevation angles too high to slip under the Es layer are just reflected into space. This is likely more of an issue for longer propagation paths, since the farther away the transmitter is from the Es layer, the smaller the range of elevations is that will actually lead to rays slipping under the Es layer.

5. Summary and conclusions

In this study, we presented an event study for 10–12 July 2012 to illustrate the effect of sporadic-E on HF radio wave propagation, and demonstrated the ability of a simple sporadic-E model to supplement a ray tracing model. For this event, radio transmissions at frequencies between 4.6 and 14.4 MHz from an HF transmitter in Qaanaaq, Greenland, received by a directional receiver in Alert, Canada, exhibited signs of transmission aided by an Es layer. Evidence included the prolonged and consistent observation of frequencies of up to 14.4 MHz, uniformly high SNR, and low received elevation angle, consistent with reflection off a 100 km altitude ionospheric layer. Such observations were not observed during the same period for the preceding and following days where a sporadic-E layer was not observed. The simplest explanation for these observations is the presence of a strong reflecting layer at E-region altitudes. These observations were confirmed by ionosonde measurements taken from a CADI instrument located in Eureka, Canada, and a Digisonde located in Qaanaaq.

A numerical ray tracer was utilized to model HF radio wave propagation through a model ionosphere with an added model Es layer in order to recreate this event. Model ionospheres were generated using E-CHAIM for 15 min intervals from 10–12 July 2012. A model sporadic-E layer consisting of a thin Gaussian disc was added to the model ionosphere at times when the Es layer was detected. Two separate versions of this model were evaluated, one using the Eureka CADI measurements to inform the Es model, and one using the Qaanaaq Digisonde measurements. In both sets of results, similar to the measured data, the results of the ray traces showed signal reception at all frequencies due to the presence of the Es layer. The effects on TOF, and most measured signal parameters other than SNR by the Es layer were replicated by the simple Es model and ray tracer. This suggests that the simple Es layer model used is sufficient for describing measured phenomena.

The effect of Es on available propagation paths were explored via ray tracing at a range of frequencies between 3 and 30 MHz. Plots of signal power versus transmitted elevation angle and frequency through an ionosphere with and without the Es showed that the addition of the Es layer allows for propagation at much higher frequencies, as long as the propagation path is short enough that the layer is over a large enough portion of the propagation path. If the propagation path is too long, the effect the layer has on the propagation paths is not necessarily beneficial.

Based on the example scenario presented, this study has shown that Es layers can significantly aid HF radio wave propagation for short ranges, by allowing for a wider range of available frequencies for propagation, and by increasing the signal power of received signals. Additionally, a simple Gaussian disc model is able to replicate these results in numerical ray traces. However, the success of this simple model does not mean that sporadic-E aided propagation paths are predictable. Since the occurrence and location of sporadic-E layers cannot easily be predicted in advance, the corresponding propagation paths cannot be predicted either. However, real-time ionosonde measurements could be used with ionospheric models to perform ray traces for current ionospheric conditions to ascertain current propagation paths available for HF radio propagation between two locations. Knowledge of the available propagation paths could eventually lead to more reliable HF radio communications, and more accurate determination of target positions with OTHR.

Declaration of competing interest

The authors declare that they have no known competing financial interests or personal relationships that could have appeared to influence the work reported in this paper.

Acknowledgements

This project was supported by TPA 02-2020 between the DRDC and NRC an under MoU 2018070005 between the DND and NRCan. HIPLAB was funded under the DRDC All Domain Situational Awareness (ADSA) program. NRCan HF transmitter network data for 2012 July 10–12 are available online at the Harvard Dataverse (https://doi.org/10.7910/DVN/YJMHKS). Infrastructure funding for CHAIN was provided by the Canada Foundation for Innovation (CFI) and the New Brunswick Innovation Foundation (NBIF). CHAIN and its operation are conducted in collaboration with the Canadian Space Agency (CSA). E-CHAIM is supported under Defence Research and Development Canada contract number W7714-186507/001/SS and is maintained by the Canadian High Arctic Ionospheric Network (CHAIN). This publication makes use of data from the Qaanaaq Digisonde, which was owned by the US Air Force Research Laboratory Space Vehicles Directorate and supported in part by the Air Force Office of Scientific Research. The authors thank Svend Erik Ascanius of the Danish Meteorological Institute and Denmark's Arctic Command for the operation of this ionosonde. The Leicester authors are grateful to the EPSRC for their support of the development of the modelling through grants EP/K008781/1, EP/C014642/1 and GR/N66056/01. This is NRCan publication number 20210241.

References

Cameron, T.G., Fiori, R.A.D., Warrington, E.M., Stocker, A.J., Thayaparan, T., Danskin, D.W., 2021. Characterization of high latitude radio wave propagation over Canada, Journal of Atmospheric and Solar-Terrestrial Physics. J. Atmos. Sol. Terr. Phys. 219 https://doi.org/10.1016/j.jastp.2021.105666.

Cannon, P., Angling, M., Barclay, L., Curry, C., Dyer, C., Edwards, R., Greene, G., Hapgood, M., Horne, R., Jackson, D., Mitchell, C., Owen, J., Richards, A., Rogers, C., Ryden, K., Saunders, S., Sweeting, M., Tanner, R., Thomson, A., Underwood, C., 2013. Extreme Space Weather: Impacts on Engineered Systems and Infrastructure. Royal Academy of Engineering, London.

Cervera, M.A., Francis, D.B., Frazer, G.J., 2018. Climatological model of over-the-horizon radar. Radio Sci. 53, 988–1001. https://doi.org/10.1029/2018RS006607.

Special topics in HF propagation. In: Coyne, V.J. (Ed.), 1979. AGARD Conf. Proc. No. 263. Advisory Group for Aerospace Research and Development, North Atlantic Treaty Organization.

Davies, K., 1990. Ionospheric Radio, IEE Electromagn, vol. 31. Ser. Peter Peregrinus, London.

Goodman, J.M., 1992. HF Communication - Science and Technology. Van Nostrand Reinhold, New York, ISBN 0-442-00145-2.
Hargreaves, J.K., 1992. The Solar-Terrestrial Environment. Cambridge University Press, Cambridge UK.
Haselgrove, J., 1963. The Hamiltonian ray path equations. J. Atmos. Terr. Phys. 25 (7), 397–399.
Huba, J.D., Krall, J., Drob, D., 2019. Global ionospheric metal ion transport with Sami3. Geophys. Res. Lett. 46, 7937–7944. https://doi.org/10.1029/2019GL083583.
Hunsucker, R.D., Hargreaves, J.K., 2003. The High-Latitude Ionosphere and its Effects on Radio Propagation, Cambridge Atmospheric and Space Science Series. Cambridge University Press, Cambridge.
ITU Recommendation P.372-15, 2021. International telecommunication union. https://www.itu.int/rec/R-REC-P.372-15-202109-I/en.
Jayachandran, P.T., Langley, R.B., MacDougall, J.W., Mushini, S.C., Pokhotelov, D., Hamza, A.M., Mann, I.R., Milling, D.K., Kale, Z.C., Chadwick, R., Kelly, T., Danskin, D.W., Cannano, C.S., 2009. Canadian high Arctic ionospheric network (CHAIN). Radio Sci. 44 (1) https://doi.org/10.1029/2008RS004046.
Jones, R.M., Stephenson, J.J., 1975. A Versatile Three-Dimensional Ray Tracing Computer Program for Radio Waves in the Ionosphere. Office of Telecommunications, OT 75-76. U.S Department of Commerce, Washington, USA.
Kirkwood, S., Nilsson, H., 2000. High-latitude sporadic-E and other thin layers - the role of magnetospheric electric fields. Space Sci. Rev. 91 (3–4), 579–613.
Technivision. In: Lied, F. (Ed.), 1967, High Frequency Radio Communications, Ed., vol. 104. AGARDograph, Maidenhead, England.
MacDougall, J.W., Jayachandran, P.T., Plane, J.M.C., 2000. Polar cap Sporadic-E: part 1, observations. JASTP 62, 1155–1167.
Newell, P.T., Greenwald, R.A., Ruohoniemi, J.M., 2001. The role of the ionosphere in aurora and space weather. Rev. Geophys. 39 (2), 137–149.
Reinisch, B.W., Galkin, I.A., 2011. Global ionospheric radio observatory (GIRO). Earth Planets Space 63, 377–381. https://doi.org/10.5047/eps.2011.03.001.
Sherstyukov, O.N., Akchurin, A.D., Ryabchenko, E. Yu, 2009. Statistical modelling of radio wave propagation under sporadic E-Layer influence. Adv. Space Res. 43, 1835–1839.
Stocker, A.J., Warrington, E.M., 2011. Nighttime sporadic E measurements on an oblique path along the midlatitude trough. Radio Sci. 46 (RS2002) https://doi.org/10.1029/2010RS004507.
Thayaparan, T., MacDougall, J., 2005. Evaluation of ionospheric sporadic-E clutter in an Arctic environment for the assessment of high-frequency surface-wave radar surveillance. IEEE Trans. Geosci. Rem. Sens. 43 (5).
Thayaparan, T., Ibrahim, Y., Polak, J., Riddolls, R., 2018. High-frequency over-the-horizon-radar in Canada. IEEE Trans. Geosci. Rem. Sens. 15 (11), 1700–1704. https://doi.org/10.1109/LGRS.2018.2856185.
Thayaparan, T., Dupont, D., Ibrahim, Y., Riddolls, R., 2019a. High-frequency ionospheric monitoring system for over-the-horizon radar in Canada. IEEE Trans. Geosci. Rem. Sens. 57 (9) https://doi.org/10.1109/TGRS.2019.2905757, 6,372-376,384.
Thayaparan, T., Marchioni, J., Kelsall, A., Riddolls, R., 2019b. Improved frequency monitoring system for sky-wave over-the-horizon radar in Canada. Geosci. Rem. Sens. Lett. IEEE 17 (4), 606–609. https://doi.org/10.1109/LGRS.2019.2928172.
Thayaparan, T., Warrington, M., Stocker, A., Siddle, D., 2020. Effect of Frequency Monitoring System for Over-the-horizon Radar Due to the Presence of Patches and Arcs within the Polar Cap Ionosphere, IRS-2020, 5-7 October 2020, Warsaw, Poland.
Thayaparan, T., Warrington, E.M., Stocker, A.J., Siddle, D.R., 2021. Simulation of the effect of convecting patches of enhanced electron density on HF over-the-horizon radars (OTHRs) in the polar regions. Geosci. Rem. Sens. Lett. IEEE. https://doi.org/10.1109/LGRS.2020.3045926.
Themens, D.R., Jayachandran, P.T., Galkin, I., Hall, C., 2017. The empirical Canadian high Arctic ionospheric model (E-CHAIM): NmF2 and hmF2. J. Geophys. Res. Space Phys. 122 https://doi.org/10.1002/2017JA024398.
Themens, D.R., Jayachandran, P.T., Bilitza, D., Erickson, P.J., Haggstrom, I., Lyashenko, M.V., et al., 2018. Topside electron density representations for middle and high latitudes: a topside parameterization for E-CHAIM based on the NeQuick. J. Geophys. Res. Space Phys. 123, 1603–1617. https://doi.org/10.1002/2017JA024817.
Themens, D.R., Jayachandran, P.T., McCaffrey, A.M., Reid, B., Varney, R.H., 2019. A Bottomside Parameterization for the Empirical Canadian High Artic Ionospheric Model (E-CHAIM), Radio Sci. https://doi.org/10.1029/2018RS006748.
Warrington, E.M., 2020. ADSA OTHR HIPLAB Software Toolbox, Contract No: W1410-195005/001/EE. Defence R&D Canada - Ottawa Research Centre, Ottawa.
Warrington, E.M., Zaalov, N.Y., Naylor, J.S., Stocker, A.J., 2012. HF propagation modeling within the polar ionosphere. Radio Sci. 47, RS0L13 https://doi.org/10.1029/2011RS004909.
Warrington, E.M., Stocker, A.J., Siddle, D.R., Hallam, J., Al-Behadili, H.A.H., Zaalov, N. Y., Honary, F., Rogers, N.C., Boteler, D.H., Danskin, D.W., 2016. Near real-time input to a propagation model for nowcasting of HF communications with aircraft on polar routes. Radio Sci. 51 (7), 1048–1059. https://doi.org/10.1002/2015RS005880.
Warrington, E.M., Stocker, A.J., Hallam, J., Siddle, D.R., Al-Behadili, H.A.H., Zaalov, N. Y., Honary, F., Rogers, N.C., Boteler, D.H., Danskin, D.W., 2017. Observations of HF radio propagation at high latitudes and predictions using data-driven simulations. In: 15th International Ionospheric Effects Symposium.
Weimer, D.R., 2005. Improved ionospheric electrodynamic models and application to calculating Joule heating rates. J. Geophys. Res. 110, A05306 https://doi.org/10.1029/2004JA010884.
Yue, X., Schreiner, W.S., Pedatella, N.M., Kuo, Y.-H., 2016. Characterizing GPS radio occultation loss of lock due to ionospheric weather. Space Weather 14, 285–299. https://doi.org/10.1002/2015SW001340.
Zaalov, N.Y., Warrington, E.M., Stocker, A.J., 2003. The simulation of off-great circle HF propagation effects due to the presence of patches and arcs of enhanced electron density within the polar cap ionosphere. Radio Sci. 38 (3), 1052 https://doi.org/10.1029/2002RS002798.
Zaalov, N.Y., Warrington, E.M., Stocker, A.J., 2005. A ray-tracing model to account for off-great circle HF propagation over northerly paths. Radio Sci. 40, RS4006 https://doi.org/10.1029/2004RS003183.
Zawdie, K.A., Drob, D.P., Siskind, D.E., Coker, C., 2017. Calculating the absorption of HF radio waves in the ionosphere. Radio Sci. 52, 767–783. https://doi.org/10.1002/2017RS006256.